nature neuroscience

A spike-timing mechanism for action selection

Catherine R von Reyn, Patrick Breads, Martin Y Peek, Grace Zhiyu Zheng, W Ryan Williamson, Alyson L Yee, Anthony Leonardo & Gwyneth M Card

We discovered a bimodal behavior in the genetically tractable organism *Drosophila melanogaster* that allowed us to directly probe the neural mechanisms of an action selection process. When confronted by a predator-mimicking looming stimulus, a fly responds with either a long-duration escape behavior sequence that initiates stable flight or a distinct, short-duration sequence that sacrifices flight stability for speed. Intracellular recording of the descending giant fiber (GF) interneuron during head-fixed escape revealed that GF spike timing relative to parallel circuits for escape actions determined which of the two behavioral responses was elicited. The process was well described by a simple model in which the GF circuit has a higher activation threshold than the parallel circuits, but can override ongoing behavior to force a short takeoff. Our findings suggest a neural mechanism for action selection in which relative activation timing of parallel circuits creates the appropriate motor output.

Although decision processes are often considered to be in the realm of higher cognition, many of our actions may be selected by more straightforward sensorimotor pathways, as suggested by studies of visual movement discrimination decision tasks in primates[1]. Invertebrate species offer a promising platform for describing sensorimotor computations in completeness at the single neuron level[2,3]. Invertebrate brains are numerically tractable, yet still exhibit hallmarks of sophisticated sensorimotor processing circuits, including feature detection[4], population coding[5], stimulus-independent[5] and value-based[6] action selection, and motor planning[7].

Historically, studies of invertebrate nervous systems have been dominated by individual large 'command' or 'command-like' interneurons that, when artificially activated, direct a specific behavioral response via either hard-wired muscle synergies[8] or control of central pattern generator networks[9]. Such circuits, which often drive rapid escape behaviors, initially promoted the notion that reflexive sensorimotor pathways underlie an invertebrate's entire behavioral repertoire. However, there is now strong evidence that this is not the case for invertebrates ranging from insects to crustaceans[10–12]. Even for time-sensitive behaviors, such as escaping a predator, more naturalistic stimuli trigger a wide range of evasive maneuvers among which the animal must actively select[3,13–15].

Flies, for example, possess a pair of large descending command interneurons, the giant fibers (GFs), whose dendrites in the central brain receive output from the optic lobes[16]. The GFs' axons traverse the fly's neck, terminating on the jump muscle motor neurons and other interneurons in the nerve cord. Artificial activation of the GFs by extracellular current injection or a light flash shown to mutant flies without eye pigment[17] drives stereotyped contraction of the fly's tergotrochanteral 'jump' muscles (TTMs) and wing-depressing dorsal lateral muscles (DLMs)[18] to trigger a takeoff[19]. Anatomical arrangement of the GFs as a direct link between sensory interneurons and motor neurons, together with their characteristic motor output, suggests that they could perform the action selection function: evaluating the visual aspect of predator approach and, when appropriate, driving a takeoff jump. For this reason, the GFs have become synonymous with *Drosophila* escape[8]. However, this role for the GFs is purely speculative because the sensory stimuli that drive the GFs remain unknown. Studies in *Drosophila* and other fly species have even suggested that a predator-like stimulus, such as a looming object, may not drive the GF to spike[20–22]. Furthermore, looming stimuli trigger a multi-stage escape sequence comprised of at least four distinct behaviors (freezing, postural adjustment, wing elevation, takeoff), a sequence that is much more elaborate than the known GF motor outputs[15]. These actions preceding the takeoff jump add crucial variability to the response. For example, they orient the fly's escape direction away from the threat[7]. Thus, it remains unknown how these more natural escape behaviors are selected and enacted by the nervous system and what role, if any, the GF circuit has.

We investigated how the timing of activity in a central neuron of the fly, the GF, selects among different escape behaviors during synthetic looming predator attacks. By analyzing over 4,000 fly escape responses recorded with high-speed video at 6,000 frames per second, we discovered that a looming stimulus triggered at least two distinct escape modes in the fly. Genetically silencing GF neurons preserved the long-mode escape, but eliminated the short-mode escape, whereas activating the GFs produced only the short mode, indicating that the GFs are necessary and sufficient for short mode escape and that other sensorimotor pathways can produce long escapes. However, when we created a head-fixed version of our behavior assay to directly record GF intracellular activity during looming-evoked escape responses, we observed GF spikes during both short- and long-mode escapes. This indicates that short and long escapes are not themselves independently controlled, but arise from the activation of a combination of sensorimotor circuits, one of which is the GF pathway. A model based on our data revealed how two independent sensorimotor pathways, each of which drives different escape action sub-components, can recreate the observed probability of selecting long and short modes

Janelia Farm Research Campus, Howard Hughes Medical Institute, Ashburn, Virginia, USA. Correspondence should be addressed to G.M.C. (cardg@janelia.hhmi.org).

Received 6 January; accepted 14 May; published online 8 June 2014; doi:10.1038/nn.3741

if they have different activation thresholds and neural delays. Finally, we recorded high-speed video of a predator, the damselfly, attacking standing *Drosophila* and found that the short-escape mode was critical for the fly to survive looming stimuli with parameters matched to the fastest of these attacks.

RESULTS

Flies select between two functionally distinct escape modes

Looming objects presumed to mimic an approaching predator elicit an escape sequence in *Drosophila* consisting of sub-behaviors such as freezing, directional posture adjustment, wing elevation and takeoff jump[15] (**Fig. 1a**). To quantify variability in the last two sub-behaviors in the sequence (wing elevation and takeoff jump), which are the most rapid, we developed a custom apparatus (**Supplementary Fig. 1**) to present a projected looming stimulus to an isolated single fly and recorded the fly's response at 6,000 frames per second. Quantifying the combined duration of the last two sub-behaviors (time from first wing elevation motion until the fly's tarsi leave the ground), we observed that, for control genotypes, the duration of this motor sequence had a multimodal distribution with at least two distinct modes (**Fig. 1b** and **Supplementary Fig. 2a**). That is, the same stimulus triggered both short ($\mu \approx 5.4$ ms) and long ($\mu \approx 13.2$ ms) escape sequences.

The short (**Fig. 1c** and **Supplementary Movie 1**) and long (**Fig. 1d** and **Supplementary Movie 2**) escape modes differed primarily in the time the fly spent elevating its wings before takeoff (**Fig. 1e**). Long-mode flies fully raised their wings (94.4% elevated their wings > 45°, $n = 355$), whereas short mode flies did not (5.6% elevated their wings >45°, $n = 95$, normal approximation to the binomial, $P << 0.001$, $Z = 17.90$), although some short-mode flies partially elevated their wings (elevation < 45°). Even without full wing elevation, flies using the short mode still executed a wing depression during the takeoff jump. This resulted in their wings being pulled further back along the abdomen during the first wing stroke than in long-mode flies (**Fig. 1c**,**d**). We previously found that the amount of time a fly uses to raise its wings correlates with steadier takeoffs and that wing-down takeoffs often cause the fly to tumble in the air during initial flight[13]. Taken together, these results indicate that, in response to a looming stimulus, flies select between two takeoff modes with different performance properties: a short mode that leads to unstable initial flight and a long mode that takes more time to complete, but produces steady flight. That is, flies trade off initial flight stability for escape sequences that are, on average, 8 ms shorter.

The percentage of flies performing short-duration escapes increased logarithmically with stimulus looming speed, as parameterized by the looming object's size-to-speed ratio, r/v (**Fig. 1f**). The size-to-speed ratio fully characterizes the pattern of retinal image size over time made by an object of half-width, r, approaching a fly directly at constant velocity, v (ref. 23). Thus, a small object approaching slowly looks the same to the fly as a large object approaching quickly if their r/v ratio is matched. For a given predator size, smaller r/v ratios indicate faster attacks. We found that the escape mode selected was not a fixed innate property of an individual fly, but was determined from a bimodal probability distribution based on the r/v ratio such that the fly is biased to select the short escape mode during faster attacks.

The GFs are necessary and sufficient to elicit short-mode escapes

The only known escape circuit in the fly is the GF pathway (**Fig. 2a**), but the stimuli that bring the GFs to threshold or whether they are involved in looming-evoked escapes remains unknown. To determine whether the GFs are involved in looming-evoked escape behavior, we use a transgenic fly line (**Fig. 2b**), constructed using previously described[24] *split-GAL4* vectors, to exclusively silence the two GFs via expression of Kir2.1 (*pJFRC49-10XUAS-IVS-eGFPKir2.1*)[24], an inwardly rectifying potassium channel[25]. We confirmed Kir2.1 expression with whole-cell GF recordings (**Supplementary Fig. 2b**). We then recorded (6,000 fps) the escape behavior in control and GF-silenced flies responding to looming stimuli.

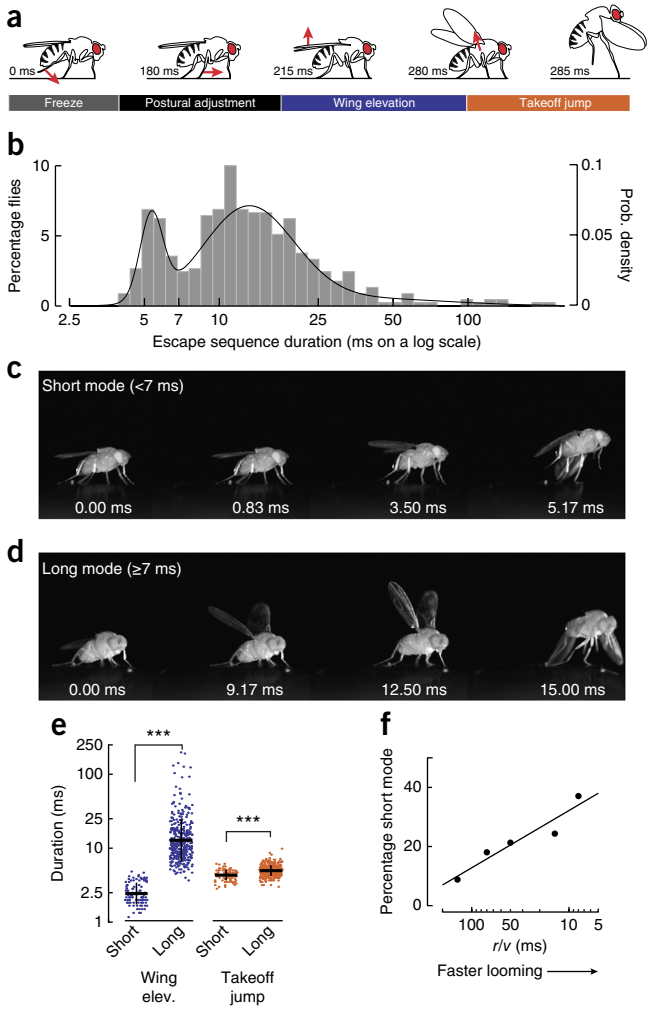

Figure 1 Flies select between two escape sequences when confronted by a looming stimulus. (**a**) The looming-evoked escape behavior sequence comprised at least four sub-behaviors. (**b**) The duration of the last two sub-behaviors, wing elevation and the takeoff jump, fitted a bimodal Gaussian distribution (control flies combined from $r/v = 14$, 40 and 70 ms trials, $n = 450$). The relative minima (6.87 ms) separated short and long escape modes. Control genotypes are *w⁺GF-split-AD UAS-Kir2.1* and *w⁺GF-split-DBD UAS-Kir2.1* (**c**,**d**) Representative video images during a short-mode (**c**) and long-mode (**d**) takeoff. (**e**) The duration of wing raising, but not jumping leg extension, was the primary contributor to the difference in duration between short- and long-mode escapes. Scatter plots show data on a log scale; black lines are mean ± s.d. (Mann-Whitney *U*, ***$P << 0.001$; short, $Z = -14.94$, $n = 95$ flies; long, $Z = -6.49$, $n = 355$). (**f**) The percentage of short-mode escapes increased with looming speed (decreasing size-to-speed ratio, r/v). The fraction of flies choosing a short-mode takeoff was negatively correlated with log(r/v) (slope = -19.27 ms^{-1}, $R^2 = 0.903$; $n = 108$, 115, 202, 133 and 102 for $r/v = 8$, 14, 40, 70 and 140 ms, respectively).

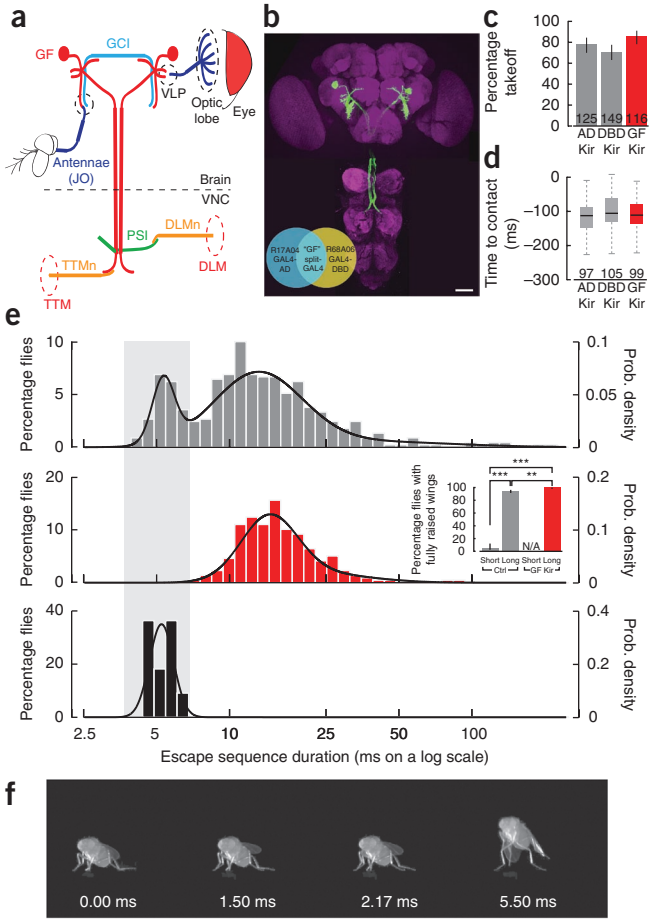

Figure 2 The GFs are necessary and sufficient for eliciting short-mode escapes. (**a**) The GF pathway. GCI, giant commissural interneurons; JO, Johnston's organ; VLP, ventrolateral protocerebrum; VNC, ventral nerve cord. (**b**) A *split-GAL4* line expressing exclusively in the GFs (green, GFP; magenta, NC82 marker for neuropil, representative image from 18 flies). Scale bar represents 50 µm. Inset, GF *split-GAL4* line intersection strategy. (**c**) GF silencing did not affect takeoff rate (r/v = 40 ms, χ^2 test, $P = 0.196$, $\chi^2 = 1.874$, n on each bar, error bars show 95% confidence interval). Control genotypes (gray bars) are as described in **Figure 1**. GF Kir: *w⁺GF-split-GAL4 UAS-myrGFP UAS-Kir2.1*. (**d**) GF silencing did not affect takeoff timing (with respect to theoretical time to contact at 0 ms; Kruskal-Wallis, $P = 0.206$, $\chi^2 = 3.161$, n under boxes). Box plots show the median (black line), 25–75th data percentiles (colored box), and 99% coverage of the data (dashed line). (**e**) The short escape mode was absent when the GFs were silenced (control flies, gray bars, n = 450; GF Kir flies, red bars, n = 218), and optogenetic stimulation of GFs expressing CsChrimson (black bars, n = 11; *w⁺GF-split-GAL4 UAS-myrGFP UAS-CsChrimson*) produced only short-mode escapes. Inset, GF-silenced takeoffs employed fully elevated wings, akin to control long-mode escapes (χ^2 test, $P << 0.001$, $\chi^2 = 80.98$, Bonferroni correction *post hoc*, $^{**}P < 0.005$, $^{***}P << 0.001$, n = 95, 355, N/A, and 218, error bars show 95% confidence interval). (**f**) Representative video frames displaying the motor sequence for optogenetic activation of GFs. The first frame (t = 0 ms) marks the first wing motion.

Although the GFs are considered to be critical for escape[8], nonfunctional GFs rendered no decrement in takeoff rate in response to the most effective escape-inducing stimuli (r/v = 14, 40 and 70 ms; **Fig. 2c** and **Supplementary Fig. 3a**). Furthermore, loss of GF function did not delay the latency to takeoff (**Fig. 2d** and **Supplementary Fig. 3b**), as might be expected after lesion of a dominant escape pathway[10].

However, when we examined the probability of flies choosing short- versus long-duration takeoffs, we found that GF silencing selectively eliminated the short escape mode (**Fig. 2e**) while preserving the long mode. The distribution of escape duration for GF-silenced flies was no longer bimodal, but was instead unimodal, with no escape duration being shorter than 7 ms, the division point between the short and long modes when the data is fit with a mixture of Gaussians. Thus, when GF activity was impaired, flies still escaped, but were limited to a long-duration escape motor program. As was characteristic of long-mode escapes in control flies, GF-silenced flies displayed full wing elevation before takeoff (**Fig. 2e**).

These results indicate the GFs are necessary for short-mode escapes. We next investigated whether they are sufficient to drive short escapes using GF activation in unrestrained flies. The GFs were previously activated in free flies[19], with the result that flies jumped with short latency to the activation. However, the *GAL4* lines used in those experiments drive expression in additional sensory or CNS neurons, and the fly's response was not observed with the temporal and spatial precision required to characterize the response as long duration or short duration[19]. Thus, it is unknown, in the context of our more detailed behavioral description, which components of escape behavior are commanded by the GFs alone. Using our GF-specific *split-GAL4* driver line, we expressed CsChrimson, a red-shifted channelrhodopsin light-activated cation channel (*UAS-CsChrimson*)[26], in only the two GF neurons. As CsChrimson requires retinal to function, experimental animals were raised on food supplemented with retinal, whereas control animals of the same genotype were given food without added retinal. Using our behavioral apparatus, we targeted single flies with four 624-nm wavelength LEDs to open CsChrimson channels. CsChrimson activation of the GFs initiated short-mode escapes with <7-ms duration (**Fig. 2e,f** and **Supplementary Movie 3**) in experimental flies (11 of 13), but not control flies (2 of 17 initiated long-duration escapes, 15 of 17 no takeoff). As expected for short-mode escapes, GF-activated takeoffs did not include full wing elevation (0 of 11 with wing elevation > 45°), although we did observed slight wing lifting (7.3 ± 2°, mean ± s.e.m., n = 9 flies) just before leg extension in some cases. We interpreted this small wing motion to be the result of indirect cuticle deformation as the TTM, the large, trans-thoracic jump muscle, starts to contract and stiffens against its dorsal attachment point before extending the leg, as suggested previously[27]. As with loom-evoked short escapes, GF-activated flies still depressed their wings during leg extension, starting the flight motor. We conclude that GF activation in free flies is sufficient to produce short mode escapes and that the GFs do not drive any active wing elevation, only a takeoff jump and flight initiation.

GF Na⁺ spikes, but not Ca²⁺-mediated potentials, drive escape

It is well-established that a single GF spike drives contraction of the fly's jump and wing depressor muscles[18]. The simplest interpretation of our results thus far is that both looming stimuli and CsChrimson activation effect at least one action potential in the GFs, initiating jump and wing muscle contraction to produce the observed short-mode takeoff actions. However, previous studies in both *Drosophila* and other fly species did not observe a GF spike in response to looming[20–22]. An alternate possibility is that the GF signaling is electrotonic. The axonal terminal of each GF interneuron makes mixed electrical and chemical synapses with both the jump muscle motorneuron (TTMn) that extends the fly's ipsilateral middle leg, and with the peripherally synapsing interneuron (PSI) that contacts the contralateral wing depressor motorneurons[8] (DLMn; **Fig. 2a**). Thus, through electrical connections, it is possible that subthreshold depolarization of the GFs could signal relevant motorneurons to trigger

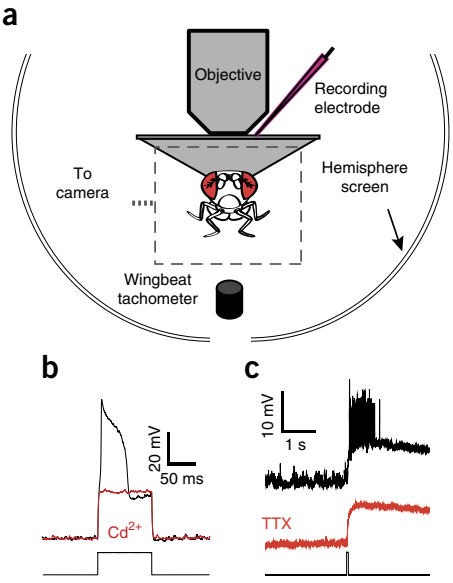

Figure 3 GF Na^+ spikes drive the short-mode escape. (**a**) A head-fixed preparation allowed simultaneous whole-cell recording from GF neurons and high-speed monitoring of escape behaviors in response to looming stimuli projected on a curved screen. (**b**) Current injection (600 pA, bottom trace) at the soma evoked large Ca^{2+}-mediated potentials (black line, representative recording from three control flies, genotype *GF-split-GAL4 UAS-GFP*) that were extinguished by application of 100 μM Cd^{2+} (red line) and did not cause escape behavior (0 of 3 flies). (**c**) ATP (1 mM, 5-ms pulse, bottom trace) stimulation of $P2X_2$ receptors expressed exclusively in the GFs evoked Na^+ spikes in the GF (black line, representative contralateral GF response from three control flies, genotype *GF-split-GAL4 UAS-GFP UAS-P2X$_2$*) that were extinguished with TTX (1 μM) and elicited escape behavior (3 of 3 flies).

jump and flight, even without the GF firing an action potential. Such electrotonic input to motorneurons has been suggested in the flight steering system of larger flies[28]. Furthermore, eliminating the chemical component of the mixed synapse does not impair the 1:1 firing of GF and TTM activation[29], whereas the TTM response is delayed and less robust in *shak-B^2* mutants that lack the electrical component of GF synapses and the DLM response is eliminated[17,30]. Both of these findings suggest that the electrical component of the mixed synapses is essential for normal function.

To investigate GF activity during looming stimuli and escape behavior, we developed a head-fixed version of our behavioral assay (a modified tethered flight preparation[31]; **Fig. 3a**) that recapitulates the observed escape behavior while allowing us to simultaneously record whole cell from GF soma. To first confirm that the muscle synergies previously reported from GF activation are synonymous with the short-mode escape that we observed, we initially tried injecting current to drive a GF spike. Somatic current injection produced large, broad regenerative potentials (reported previously[32]) that did not result in any escape behaviors (0 of 3 flies). These regenerative potentials resembled Ca^{2+}-dependent potentials that modulate spike bursting[33]. Bath application of Cd^{2+} to block voltage-gated Ca^{2+} channels inhibited the potentials, suggesting they are indeed Ca^{2+} mediated (**Fig. 3b**).

Given that the soma of insect neurons is distal from the spike initiation zone, somatic stimulation may not mimic dendritic current influx[34]. We instead stimulated the GF using GF-restricted expression of ionotropic, ATP-gated $P2X_2$ receptors[19] and micro-injections of ATP along the GF dendrites. Unlike our CsChrimson activation, this allowed unilateral activation of a single GF and better mimicked dendritic activation. Small ATP pulses (<5 psi) caused only subthreshold GF responses and did not evoke any escape behavior (3 of 3 flies). However, stronger pulses (5 psi) on either ipsi- (**Supplementary Fig. 4a**,**c**) or contralateral (**Fig. 3c** and **Supplementary Fig. 4b**) sides elicited a train of narrower spikes and the expected behavioral output: a short-mode takeoff consisting of leg extension (7 of 7 flies), wing depression without preceding wing elevation (7 of 7 flies) and flight initiation (4 of 7 flies). The lower rate of flight initiation may be attributed to the unnaturally long GF spike train induced by our stimulation causing prolonged muscle contraction, which hampers the oscillating flight motor in some cases. Bath application of tetrodotoxin (TTX) to block voltage-gated Na^+ channels eliminated both GF spikes (**Fig. 3c** and **Supplementary Fig. 4c**,**d**) and the behaviors (6 of 6 flies). Thus, we found that the GF is able to produce at least two different types of active potentials: broad Ca^{2+}-mediated potentials driven by current influx at the soma and narrow Na^+ potentials requiring current influx at the dendrites.

We suggest that the most parsimonious explanation for our results, together with previous observations of the mixed GF-TTMn synapse, is that GF dendritic activation sufficient to evoke Na^+ spikes is required to drive a jump and flight-initiating downstroke, but does not cause wing elevation. Subthreshold, electrotonic signals and Ca^{2+}-mediated potentials are not sufficient alone to drive behavior, although we cannot preclude the possibility that they traverse GF-TTMn and GF-PSI gap junctions to summate with other excitatory inputs and initiate takeoff.

Naturalistic looming stimuli drive GF spikes during both modes

We next recorded whole-cell from the GF soma while observing tethered escape responses to looming stimuli (**Fig. 3a**). Both ipsi- and contralateral looming stimuli elicited one or two GF spikes per loom in a subset of flies (10 of 33 flies; **Fig. 4a**, **Supplementary Fig. 5** and **Supplementary Movies 4–6**). The spikes occurred with similar latency from stimulus onset as takeoffs in freely behaving flies (**Fig. 4b**), indicating that the timing of the response is comparable to unrestrained escapes. As in our direct activation experiments, each GF spike was followed by rapid extension of the fly's middle (jumping) legs and flight initiation with short, stereotyped latencies (0.9 ± 0.2 ms and 2.0 ± 0.1 ms, respectively; 27 of 27 trials in 5 of 5 flies; **Fig. 4a**,**c**). These latencies were similar to those reported from GF spike to jump and wing depressor muscle potentials (TTM, 0.81 ± 0.07 ms; DLM, 1.25 ± 0.10 ms)[18], indicating that our observed behavior is synonymous with known GF-driven muscle activation. In contrast, elevation of the wings commenced with variable latency before GF spikes (**Fig. 4c**), further confirming that the GFs are not involved in this component of the behavior.

In an overlapping subset of flies (9 of 33 flies), looming stimuli evoked flight initiation without GF spiking. This confirms there must be alternate, non-GF, descending pathways connecting visual information from the optic lobes with flight muscles in the fly's thorax that initiate flight in response to looming. In these cases, we did not detect a jump (no mesothoracic leg extension). As we never observed the fly to initiate flight without prior leg extension in free behavior experiments, we hypothesize that cues missing from the tethered preparation, such as tarsal contact, may be necessary to engage the non-GF circuit(s) for jumping.

If, as our results suggest, a GF spike drives the short escape mode in response to looming stimuli, whereas non-GF circuits mediate the long escape mode, then we expect that looming stimuli will drive a spike in the GF just before short, but not long, mode tethered takeoffs.

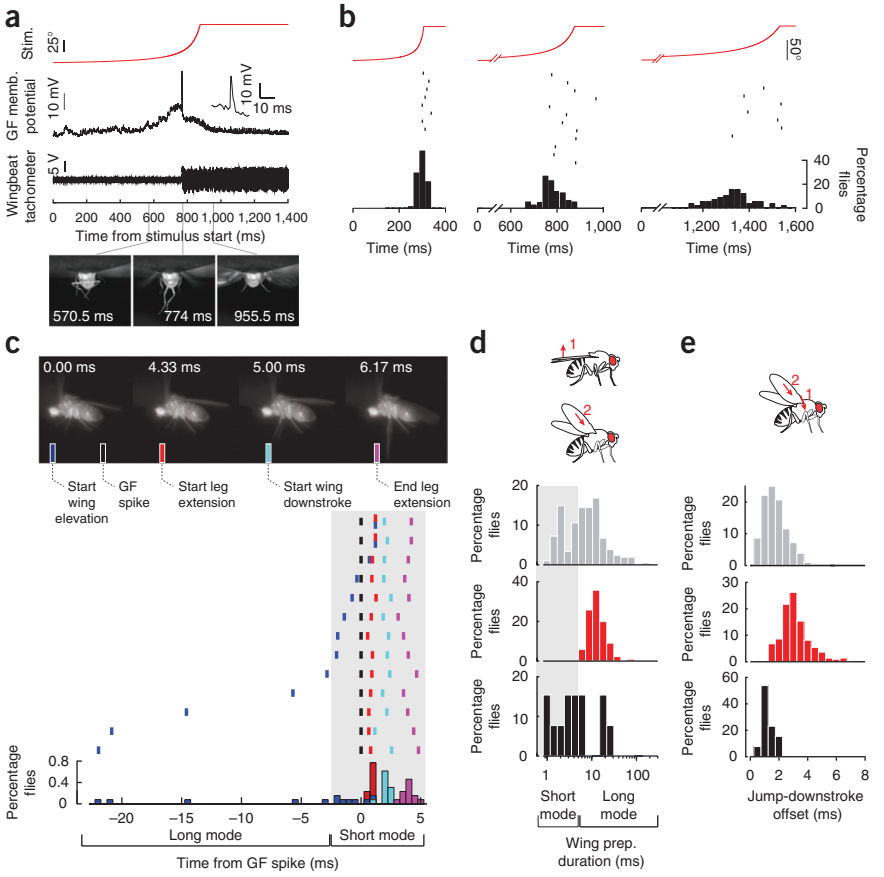

Figure 4 GF spike timing determines escape mode. (**a**) Example loom-evoked GF spiking trial. Middle leg extension (jump) and flight initiation immediately follow the spike. Top, retinal stimulus size; second row, GF membrane potential; third row, wingbeat tachometer; bottom, high-speed video images; inset, expanded spike trace. (**b**) GF spikes occurred with similar latency to looming as takeoffs in free behavior trials. Top, stimulus size; second row, rasters of first GF spike (27 trials, 10 flies); third row, distribution of free behavior takeoff latency (n = 77, 72 and 59 flies for r/v = 14, 40 and 70, respectively). (**c**) Timing of escape sub-behaviors relative to GF spike. Top, example video frames illustrating escape components; middle row, behavior rasters marking time each behavior occurred relative to GF spike (13 trials, 5 flies); bottom, distributions of behavior timings. Wing raising time was not conserved relative to GF spikes, and GF spiking trials include both long-mode (white area) and short-mode (gray area) escapes. (**d**) Distribution of wing raising duration (start of wing raising to start of first downstroke) for loom-evoked takeoffs in unrestrained control flies (gray, n = 208 flies, r/v = 14, 40 and 70 combined), unrestrained GF-silenced flies (red, n = 218 flies) and head-fixed GF spiking trials (black, 13 trials, 5 flies). Gray area indicates trials falling into the short mode, as in **c**. (**e**) Distribution of the offset between the start of leg extension and the start of the wing downstroke for looming evoked takeoffs. Data are presented as in **d**. Genotypes: *w⁺GF-split-GAL4 UAS-GFP* (electrophysiology), *w⁺ GF-split-GAL4 UAS-myrGFP* (free behavior).

We therefore measured the duration of the tethered escape sequence from the start of wing elevation to the start of flight. To our surprise, although wing raising duration was significantly shorter in trials with GF spikes compared with those without ($\mu = 7.4 \pm 2.3$ and 15.7 ± 3.6 ms, n = 13 and 6 trials across 5 and 6 flies, Mann Whitney U, P = 0.034, U = 106), GF spikes were not confined to short escapes, but also included some long escapes in which the fly had time to fully elevate its wings (5 of 13 trials >7 ms; **Fig. 4c**). Comparison of free behavior and physiology data therefore suggests that short-mode escapes require the GF pathway (they occur with GF spikes and are absent without them), whereas long-mode escapes may use multiple pathways, including the GF (they occur both in the presence and absence of GF spikes; **Fig. 4c**,**d**).

We also observed that only the GF pathway drove escapes with the shortest latency in a specific behavioral interval: the time between the start of leg extension and wing depression (jump-downstroke offset, **Fig. 4e**). This stereotyped motor act was predicted from the hard-wired motor outputs of the GF circuit (**Fig. 2a**), and is evidence against complete redundancy in motor control: even degenerate pathways that appear to have the same higher order output, such as takeoff, may have a unique signature.

GF spike timing determines the escape mode

The occurrence of GF spikes during both short and long escapes suggests that the two escape modes are not simply distinguished by GF participation. Our data can be explained by a system in which the presence and timing of a GF spike, with respect to the activation of non-GF circuit(s) that start elevation of the wings and control non-GF takeoffs, determines whether the fly produces a long- or short-mode escape. Under this hypothesis, one expects the GF and non-GF pathways must be differentially activated by a looming stimulus, either as a result of a different threshold of activation or a different delay to activation. We investigated whether this was true in our behavioral data by looking at the response times of three different groups of flies to looms: control flies exhibiting short (<7 ms) escapes, which we infer from our silencing and physiology data must all be GF-mediated responses, control flies exhibiting long (≥7 ms) escapes, which we infer are primarily non-GF mediated, and GF-silenced escapes (all ≥7 ms), which must be non-GF mediated (**Fig. 5a**).

The response time of looming detection circuits and their concomitant behaviors have been shown to follow a linear relationship across a range of looming stimulus size-to-speed ratios[21,23,35,36]. As r/v decreases (rate of expansion increases), an animal has less time to respond, so both peak firing rate of loom-responsive neurons and behavior occur closer to time of contact (TOC), the time at which the stimulus theoretically reaches 180° retinal size and therefore contacts the animal[23]. In accordance with other looming systems, we found the timing of both wing elevation and takeoff to be linearly related across three r/v ratios in the range eliciting the most short-mode escapes (**Fig. 4a**). In this range, timing of control long-mode and GF-silenced behaviors were not significantly different (**Fig. 4a**), suggesting GF absence does not alter the response time of long-mode behaviors. Both, however, varied significantly from short-mode escapes in slope (ANCOVA; wings: P = 0.0191, F = 19.48; takeoffs: P = 0.0046, F = 52.73; Tukey's HSD *post hoc*), and time of wing elevation and takeoff at specific r/v ratios (**Fig. 5a**).

Differences in timing between short versus long and GF-silenced escapes suggest that GF and non-GF escapes may use different

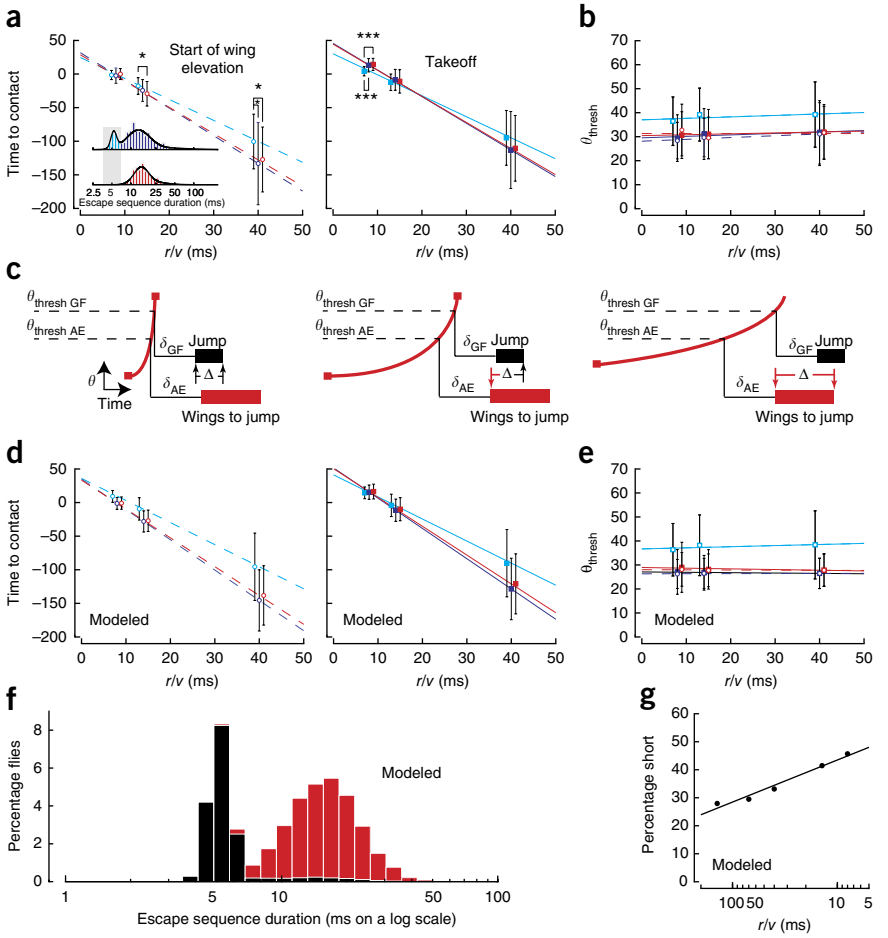

Figure 5 A dual-circuit, angular size threshold model recapitulates the timing and selection between short- or long-mode escape. (**a**) Time of wing elevation (circles, mean ± s.d.; dashed lines, linear fit) or takeoff (squares, solid lines) across r/v for control flies using short-mode (cyan, $n = 40$, 28, 43 for $r/v = 8$, 14 and 40 ms) or long-mode takeoffs (blue, $n = 68$, 87 and 159) and GF-silenced flies (GF Kir, red, $n = 57$, 58 and 99); $R^2 > 0.99$ for all fits. Short-mode timings differed significantly from those of GF Kir flies (Kruskal-Wallis, $P = 0.8579$, 0.0246, 0.0062 for wing raising, 0.0006, 0.9694, 0.1254 for takeoff; $\chi^2 =$ 0.307, 7.410, 10.17 wings, 14.77, 0.062, 4.153 takeoff at $r/v = 8$, 14 and 40 ms, respectively; $^*P < 0.05$, $^{***}P < 0.001$, Tukey's HSD *post hoc*). (**b**) Stimulus size (mean ± s.d.) at a fixed neural delay preceding takeoff or wing elevation was invariant across r/v (slope not significantly different from zero, linear regression t test, $P = 0.5524$, 0.2029 and 0.9997 wings, 0.5456, 0.3707 and 0.0781 takeoffs; $t = 0.8475$, 3.031 and −0.0005 wings, 0.866, 1.519 and 8.106 takeoffs for short, long and GF-silenced fits, respectively). (**c**) To determine escape response duration (Δ), we modeled behavior driven by either GF or alternate escape (AE) pathways with a fixed delay after the stimulus size threshold. This can yield either a GF-mediated short escape (left), GF-mediated escape interrupting wing raising (middle) or long escape without GF involvement (right). (**d**–**g**) This model recapitulates the behavior timing (mean ± s.d., **d**), size threshold (mean ± s.d., **e**), bimodal distribution of takeoff duration (**f**) and log-linear increase in short-mode usage across r/v (**g**) observed in the experimental data ($n = 5{,}000$ modeled control or GF Kir flies; $R^2 > 0.999$ for all fits in **d**; slopes in **e** not significantly different than 0, linear regression t test, $P = 0.4152$, 0.7859, 0.7950 wings, 0.4156, 0.1567, 0.2125 takeoffs, $t = 0.2729$, −1.256, −1.332 wings, 0.2715, 1.865, 1.269 takeoffs for short, long, and GF Kir fits, respectively; in **g**, slope = −15.83, $R^2 = 0.96$).

stimulus features or thresholds to gate their respective behaviors. To evaluate these potential differences, we applied a size threshold model previously established for looming detector circuits[23,35]. In this model, behavior is initiated at a fixed neural delay after a looming stimulus crosses an angular size threshold on the retina. These assumptions predict a linear relationship between behavioral timing and r/v, just as we found for our data. Under this model, the y intercept of the fit represents an estimation of the neural delay. One can think of it as the extrapolated response latency to an infinitely fast, or instantaneous, loom. Estimated neural delays for wing elevation were 24.6, 31.7 and 28.6 ms for short, long and GF-silenced escapes, respectively. Neural delays for takeoff were larger than those for wing elevation, and the differences between the delays (5.6, 14 and 15.9 ms for short, long and GF-silenced escapes) were similar to mean measured escape durations (5.4, 13.2 and 14.6 ms). Short escapes, however, had a smaller neural delay to takeoff (30.1 ms) than long (45.7 ms) or GF-silenced (44.5 ms) escapes, suggesting that GF-mediated takeoffs have the shortest neural delay from photoreceptor input to motor neuron output.

To test for the existence of an angular size threshold, we plotted the retinal stimulus size when the wing-elevation or takeoff pathways were triggered, given the estimated neural delay (**Fig. 5b**). In all cases, the data fit a linear model with a slope that was not significantly different from zero, indicating an invariant angular threshold across r/v (**Fig. 5b**). The thresholds for short mode behaviors were significantly larger than those for long or GF-silenced escapes ($r/v = 8$, 14 and 40; Kruskal-Wallis, wings: $P = <<0.0001$, $<<0.0001$, 0.0004, $\chi^2 = 20.29$, 19.01, 15.47; takeoffs: $P = 0.0002$, 0.0005, 0.0016, $\chi^2 = 16.79$, 15.24, 12.86; Tukeys HSD *post hoc*; **Fig. 5b**), suggesting the GF pathway has a shorter neural delay, but a higher activation threshold to drive an escape behavior. We also found that, in short, long and GF-silenced groups, the size threshold was not significantly different for wing elevation versus takeoff behaviors (Wilcoxon rank sum; short, $P = 0.9667$, $Z = -0.0418$, $n = 111$; long, $P = 0.6127$, $Z = 0.5063$, $n = 314$; GF silenced, $P = 0.6775$, $Z = -0.4158$, $n = 214$). This was expected for GF-mediated short escapes, as the small movement of the wings before leg extension directly results from the activation of the GF circuit. However, this result highlights a dependency between wing elevation and takeoff for non-GF escapes and suggests that only one additional sensorimotor circuit may be required to direct wing elevation and a non-GF takeoff. Thus, our data suggest that the observed bimodal distribution of escape behavior duration results from two parallel circuits, one that drives a GF takeoff and another that drives wing elevation and takeoff after completion of wing elevation.

We next investigated whether a two-circuit, angular threshold model could predict both the timing and behavioral selection seen in freely behaving flies. As an input to this model, we used normal or log normal distributions fit to the angular size threshold (Online Methods and **Supplementary Fig. 6**) and escape behavior duration

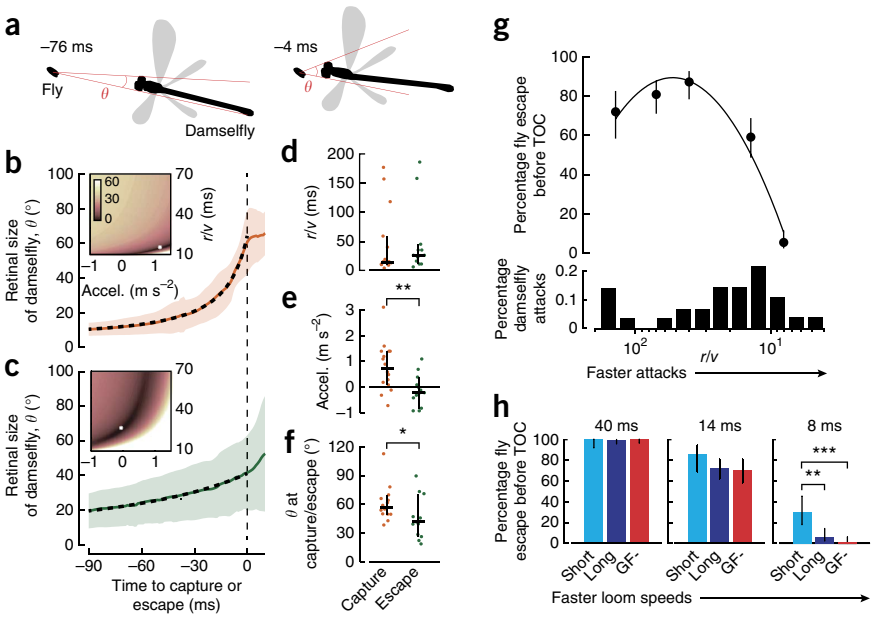

Figure 6 GF-mediated short escapes confer a survival advantage within an ethologically relevant regime. (**a**) Relative damselfly and fly positions in example video frames during an attack (milliseconds before fly capture). (**b**,**c**) Damselfly size on the fly's eye (mean ± s.d.) during attacks leading to fly capture (**b**, $n = 16$) or escape (**c**, $n = 13$). Dashed black line is best-fit model using initial size-to-speed ratio (r/v) and acceleration (a) parameters with the smallest residual (white asterisk, inset, Online Methods). (**d**–**f**) Model values (median ± 95% confidence interval) for r/v, acceleration and final damselfly size on fly retina at time of capture/escape for model fit to individual damselfly trajectories (Wilcoxon rank sum test, $^*P < 0.05$, $^{**}P < 0.005$, $Z = -1.076$, 2.832 and 2.208 for r/v, acceleration, and final size, respectively). Median acceleration was significantly different from 0 for capture (signed rank test, $P < 0.005$, $Z = 2.82$), but not escape events (signed rank test, $Z = -0.7851$, $P = 0.46$). (**g**) Expected survival rate (percentage of flies taking off before theoretical time of contact, TOC) for wild-type flies across simulated predator attack speeds (expressed as r/v) and the distribution of observed damselfly attack size-to-speed ratios ($n = 50$, 83, 85, 88 and 107 for r/v values of 140, 70, 40, 14 and 8 ms respectively). (**h**) Short-mode takeoffs confer a significantly higher survival rate (takeoff initiated before TOC) during fast looms (control fly short-mode escapes, cyan; long-mode escapes, blue; GF Kir fly escapes, red; χ^2 test, $P = 0.365$, 0.531 and 0.0004; $\chi^2 = 2.041$, 1.268, 15.70 for $r/v = 40$, 14 and 8 ms, respectively, Bonferroni correction *post hoc*, $^{**}P < 0.005$, $^{***}P < 0.001$). Error bars in **g** and **h** represent 95% confidence intervals.

(from **Fig. 2e**) in cases in which only the GF was active (GF loom-evoked spiking trials and GF CsChrimson activation) and in cases in which only the non-GF circuits were active (GF-silenced Kir trials). We then simulated a fly's response to a looming stimulus by randomly drawing from the modeled distributions an angular threshold and behavioral duration for the GF and non-GF circuit (**Fig. 5c**). Both the GF and non-GF circuits could mediate the takeoff jump. Our model chose the circuit with the earliest takeoff response as the 'winning' pathway. This meant the GF circuit could interrupt the wing elevation portion of the non-GF pathway response, shortening the normal response duration of that pathway and resulting in some GF-mediated escapes with durations longer than GF activation alone (**Fig. 5c**).

We found that this model recapitulated wing and takeoff timing (**Fig. 5d**,**e**) and the bimodal distribution in escape behavior duration (**Fig. 5f**). A small subset of GF-driven escapes fell into the long duration category, similar to the behavior observed during whole-cell GF recordings. Notably, the model also recapitulated the linear increase in the bias to utilize more GF short escapes with increasing predator speed (decreasing r/v, **Fig. 5g**). As predation velocity increases, the elapsed time between looming cues crossing the two size thresholds decreases, so that the wining pathway becomes the one with the shortest neural delay. This suggests that the GFs may provide an advantage in the presence of rapidly approaching predators, by having both a short neural delay to initiate an escape behavior and the ability to shorten the duration of the behavior.

GF short-mode escapes enhance survival from rapidly approaching predators

To test the possibility that the GF circuit conveys a survival advantage during rapid predator approaches, we measured attack trajectories of damselflies preying on *Drosophila*, quantifying the visual cues of natural predation events. We tracked damselflies in three dimensions at 1,000 frames per second as they preyed on flies in a naturalistic environment. Damselflies first positioned themselves at the same height as a fly standing on a vertical wall, then darted forward (peak speed of 0.65 m s^{-1}) and grabbed the fly with all six legs. This flight path creates a looming stimulus on the fly's eye (**Fig. 6a**) and is the primary visual stimulus that might drive an escape response.

To fit the time course of this looming nonlinear expansion, we used the damselfly acceleration and r/v value at the moment an attack started as parameters in a model of predator approach for two types of damselfly attack trajectories: those resulting in capture (**Fig. 6b** and **Supplementary Movie 7**) and those from which the fly escaped (Online Methods, **Fig. 6c** and **Supplementary Movie 8**). Initial r/v values for capture and escape trajectories were not significantly different (rank sum test, $P = 0.28$; **Fig. 6d**), but capture trajectories had positive acceleration, whereas escape trajectories were, on average, constant velocity (signed rank test comparison to 0; capture, $P = 0.0048$; escape, $P = 0.46$; **Fig. 6e**). We also found that damselflies loomed to a larger final size on the fly's retina for capture events than for escapes (rank sum test, $P = 0.027$; **Fig. 6f**).

These studies confirmed looming stimuli as a reasonable proxy for visual cues during a predator attack on *Drosophila*. We found that damselflies attack *Drosophila* with a wide variety of approach trajectories. *Drosophila* escape circuits are most responsive to the slower, constant-velocity approaches, whereas accelerating attacks that end at high velocity are more difficult for the fly to detect.

We next projected constant-velocity looming stimuli across the full r/v range observed in the damselfly predation data (8–140 ms; **Fig. 6g**) to flies in our behavioral apparatus and measured their expected survival rates (percentage of flies taking off before the theoretical time of contact, TOC). We found that fly 'survival' rates were lowest for stimuli that modeled the fastest, and most common, damselfly attack speeds (**Fig. 6g**). This suggests that damselflies attack *Drosophila* at speeds near the edge of the fly's ability to respond in time and indicates that the 8-ms average difference we measured between the fly's short- and long-mode escapes could, in fact, make the difference between life and death.

To test this directly, we looked at whether the survival mode chosen by the fly affected its predicted survival rate and whether GF-silenced

flies, who are unable to execute short escapes, were at a disadvantage. For projected looming stimuli representing slower damselfly attacks ($r/v = 40$), we found no significant survival difference between short-mode, long-mode and GF-silenced escapes (**Fig. 6h**). However, for looming stimuli closer to maximum damselfly attack performance ($r/v = 8$ ms), flies using a short escape were significantly more likely to survive (30% takeoff before TOC at $r/v = 8$ ms) than those employing a long escape or those with silenced GFs (6% and 0% takeoff before TOC at $r/v = 8$ ms, respectively, χ^2 test, $P = 0.0004$, $\chi^2 = 15.70$). These results suggest that the GFs do indeed confer a competitive advantage when a predator rapidly approaches.

DISCUSSION

We observed previously unknown flexibility in *Drosophila* escape behavior and found that it arises from parallel activation of at least two separate descending motor pathways that drive an escape in response to identical visual cues. One of these pathways includes the GFs, known command neurons for jump takeoff, and the other does not. A model based on our data suggests that these two circuits have overlapping tuning to visual cues of predator approach, but differences in their activation thresholds and neural delays produce the observed escape motor program flexibility. Consequently, flies are able to select between rapid, but unsteady, or slow, but stable, takeoffs when escaping an approaching predator.

Previously, studies of rapid escape behaviors have attributed variability in escape responses to stimulus variability. For example, stimulus direction can explain escape direction[7,10] and stimulus modality[10,37] or abruptness[10] can correlate with behavioral latency or type of response. We eliminated stimulus variability by presenting identical looming profiles at the same location relative to a freely moving fly in repeated trials. These experiments were then corroborated with head-fixed trials in which the retinal location of the stimulus was repeated exactly. Thus, we attribute our observed variability in escape motor program durations to internal sources, represented in our model as noise around the size threshold for each escape circuit. The observed variability arises from the overlapping noisy probability of activating each of the escape pathways.

Our data indicate that at least two escape circuits transform sensory information into motor commands in response to identical visual stimuli. Such parallel sensorimotor processing may be a conserved principle for action selection across species[38]. For example, neural representations of multiple, potential motor actions occur before action selection in primate sensorimotor tasks[39–41]. Multiple circuits for escape have also been identified in other species, including the lateral giant, medial giant and non-giant circuits of the crayfish[3,10], three looming-sensitive pathways in the locust (DCMD, DIMD and LDCMD)[42–44], and the Mauthner cell network of teleost fish and tadpoles[45]. Although some of these pathways may be recruited serially[3], there is also evidence for parallel activation. For example, in response to certain stimuli, both the Mauthner cell and its homologs show elevated Ca^{2+} activity[37,46].

We utilized the *Drosophila* genetic toolkit to manipulate single neurons in fully intact, behaving flies to supply the most direct evidence to date that parallel processing occurs during natural escape behavior in response to ethologically relevant stimuli and provides a survival advantage for the animal. In an ethological context, parallel processing may be more advantageous than serial decision-making, as it enables an animal to quickly engage alternate motor actions when sensory cues change rapidly in a natural environment[38]. This is illustrated particularly well here in *Drosophil*a escape. As a threat looms, flies engage the GF pathway with increasing probability. Once activated, the GF pathway interrupts any escape sequence initiated through alternate pathways. A similar kind of override has been observed during fish escape when Mauthner cell activation overrides swimming CPGs to quickly transition a fish from swimming to escape[47]. Based on our model, we hypothesize that this interrupt could occur, without requiring lateral inhibition of parallel motor control pathways, directly at the level of the musculature of the fly, where the engagement of the leg extensor and wing depressor muscles through GF activation could be strong enough to overcome the driving force of any other behavior command. In this case, reciprocal inhibition between the motor pathways[47] would not be required to select the appropriate action.

The often-stated purpose of giant neuron escape circuits is to initiate escape behavior with the shortest latency from stimulus onset[10] via high conduction velocities of large-diameter axons[48]. Consistent with this idea, the neural delays that we estimated for the GF circuit were smaller than those of alternate escape circuits, and the behavior driven following direct GF activation is of the shortest duration seen in response to looming stimuli. However, we found that a short neural delay and behavior duration does not necessarily translate to the fastest response from stimulus onset for naturalistic stimuli. Although in response to fast-looming attacks (small r/v), GF-mediated, short-duration escapes occurred substantially earlier than other escapes, for slow-looming attacks (large r/v), they occurred later because of the higher angular size activation threshold of the GF compared with alternate pathways. In addition, GF spiking often followed other components of the takeoff behavior, including wing elevation. We suggest that the benefit realized from having a GF circuit is not to initiate, but to reliably complete the escape sequence in the shortest amount of time. This makes sense from an ecological perspective, as selection pressure from predators likely favors individuals able to get away fastest, not those that merely have a fast reaction time.

Our results establish the role of GFs in the natural ecology of *Drosophila*. The data support the existence of alternate pathways that can mediate takeoff behaviors in flies[21,49,50]. Our results therefore provide a platform with which to investigate whether and how parallel representations exist in real time. Future work should take advantage of *Drosophila* escape behavior as a genetically tractable model for understanding how sequential motor outputs are organized through parallel circuits to produce a coordinated, but flexible, behavior.

METHODS

Methods and any associated references are available in the online version of the paper.

Note: Any Supplementary Information and Source Data files are available in the online version of the paper.

ACKNOWLEDGMENTS

We thank T. Ngo and A. Jenett (Janelia Farm Research Campus) for providing the *GF-split GAL4* line, B.D. Pfeiffer (Janelia Farm Research Campus) for *pJFRC12-10XUAS-IVS-myr::GFP*, *pJFRC28-10XUAS-IVS-GFP*, and *pJFRC49-10XUAS-IVS-eGFPKir2.1* flies, and K. Wantanabe (Caltech) for the *pUAS-EGFP-Kir2.1* DNA. We thank V. Jayaraman and A. Karpova (Janelia Farm Research Campus) for providing *UAS-CsChrimson* flies. We thank P. Herold for damselfly husbandry and assistance with data collection and R. Franconville for help troubleshooting $P2X_2$ receptor experiments. We thank V. Jayaraman, G. Murphy and S. Huston for their comments on the manuscript. We thank the Janelia Fly Facility (T. Laverty, A. Cavallaro, K. Hibbard, D. Hall, M. Mercer, D. Fetter, J. McMachon, J.-C. Kao and D. Ruiz). We thank the Janelia Instrument Design and Fabrication Department for help with the behavioral apparatus.

AUTHOR CONTRIBUTIONS
C.R.v.R., A.L. and G.M.C. prepared the paper. C.R.v.R., P.B. and G.M.C. analyzed data. C.R.v.R., P.B., W.R.W. A.L.Y. and G.M.C. performed experiments. C.R.v.R., A.L. and G.M.C. designed experiments. G.Z.Z. provided genetic tools. C.R.v.R. built the electrophysiology apparatus. M.Y.P., W.R.W. and G.M.C. built the behavioral apparatus. A.L. built the damselfly tracking system.

COMPETING FINANCIAL INTERESTS
The authors declare no competing financial interests.

1. Gold, J.I. & Shadlen, M.N. The neural basis of decision making. *Annu. Rev. Neurosci.* **30**, 535–574 (2007).
2. Kristan, W.B. Neuronal decision-making circuits. *Curr. Biol.* **18**, R928–R932 (2008).
3. Herberholz, J. & Marquart, G.D. Decision making and behavioral choice during predator avoidance. *Front. Neurosci.* **6**, 125 (2012).
4. Seelig, J.D. & Jayaraman, V. Feature detection and orientation tuning in the *Drosophila* central complex. *Nature* **503**, 262–266. 10.1038/nature12601 (2013).
5. Briggman, K.L., Abarbanel, H.D. & Kristan, W.B. Jr. Optical imaging of neuronal populations during decision-making. *Science* **307**, 896–901 (2005).
6. Zhang, K., Guo, J.Z., Peng, Y., Xi, W. & Guo, A. Dopamine-mushroom body circuit regulates saliency-based decision-making in *Drosophila*. *Science* **316**, 1901–1904 (2007).
7. Card, G. & Dickinson, M.H. Visually mediated motor planning in the escape response of *Drosophila*. *Curr. Biol.* **18**, 1300–1307 (2008).
8. Allen, M.J., Godenschwege, T.A., Tanouye, M.A. & Phelan, P. Making an escape: development and function of the *Drosophila* giant fibre system. *Semin. Cell Dev. Biol.* **17**, 31–41 (2006).
9. Wiersma, C.A. & Ikeda, K. Interneurons commanding swimmeret movements in the crayfish, *Procambarus clarkii* (Girard). *Comp. Biochem. Physiol.* **12**, 509–525 (1964).
10. Edwards, D.H., Heitler, W.J. & Krasne, F.B. Fifty years of a command neuron: the neurobiology of escape behavior in the crayfish. *Trends Neurosci.* **22**, 153–161 (1999).
11. Harley, C.M., English, B.A. & Ritzmann, R.E. Characterization of obstacle negotiation behaviors in the cockroach, *Blaberus discoidalis*. *J. Exp. Biol.* **212**, 1463–1476 (2009).
12. Ofstad, T.A., Zuker, C.S. & Reiser, M.B. Visual place learning in *Drosophila melanogaster*. *Nature* **474**, 204–207 (2011).
13. Card, G. & Dickinson, M.H. Performance trade-offs in the flight initiation of *Drosophila*. *J. Exp. Biol.* **211**, 341–353 (2008).
14. Hemmi, J.M. & Tomsic, D. The neuroethology of escape in crabs: from sensory ecology to neurons and back. *Curr. Opin. Neurobiol.* **22**, 194–200 (2012).
15. Card, G.M. Escape behaviors in insects. *Curr. Opin. Neurobiol.* **22**, 180–186 (2012).
16. Bacon, J.P. & Strausfeld, N.J. The dipteran 'Giant fiber' pathway - neurons and signals. *J. Comp. Physiol. A Neuroethol. Sens. Neural Behav. Physiol.* **158**, 529–548 (1986).
17. Thomas, J.B. & Wyman, R.J. Mutations altering synaptic connectivity between identified neurons in *Drosophila*. *J. Neurosci.* **4**, 530–538 (1984).
18. Tanouye, M.A. & Wyman, R.J. Motor outputs of giant nerve fiber in *Drosophila*. *J. Neurophysiol.* **44**, 405–421 (1980).
19. Lima, S.Q. & Miesenbock, G. Remote control of behavior through genetically targeted photostimulation of neurons. *Cell* **121**, 141–152 (2005).
20. Holmqvist, M.H. A visually elicited escape response in the fly that does not use the giant fiber pathway. *Vis. Neurosci.* **11**, 1149–1161 (1994).
21. Fotowat, H., Fayyazuddin, A., Bellen, H.J. & Gabbiani, F. A novel neuronal pathway for visually guided escape in *Drosophila melanogaster*. *J. Neurophysiol.* **102**, 875–885 (2009).
22. Mu, L., Ito, K., Bacon, J.P. & Strausfeld, N.J. Optic glomeruli and their inputs in *Drosophila* share an organizational ground pattern with the antennal lobes. *J. Neurosci.* **32**, 6061–6071 (2012).
23. Gabbiani, F., Krapp, H.G. & Laurent, G. Computation of object approach by a wide-field, motion-sensitive neuron. *J. Neurosci.* **19**, 1122–1141 (1999).
24. Pfeiffer, B.D. *et al.* Refinement of tools for targeted gene expression in *Drosophila*. *Genetics* **186**, 735–755 (2010).
25. Baines, R.A., Uhler, J.P., Thompson, A., Sweeney, S.T. & Bate, M. Altered electrical properties in *Drosophila* neurons developing without synaptic transmission. *J. Neurosci.* **21**, 1523–1531 (2001).
26. Klapoetke, N.C. *et al.* Independent optical excitation of distinct neural populations. *Nat. Methods* **11**, 338–346 (2014).
27. Levine, J. & Tracey, D. Structure and gunction of giant motorneuron of *Drosophila melanogaster*. *J. Comp. Physiol.* **87**, 213–235 (1973).
28. Fayyazuddin, A. & Dickinson, M.H. Haltere afferents provide direct, electrotonic input to a steering motor neuron in the blowfly, Calliphora. *J. Neurosci.* **16**, 5225–5232 (1996).
29. Fayyazuddin, A., Zaheer, M.A., Hiesinger, P.R. & Bellen, H.J. The nicotinic acetylcholine receptor Dalpha7 is required for an escape behavior in *Drosophila*. *PLoS Biol.* **4**, e63 (2006).
30. Allen, M.J. & Murphey, R.K. The chemical component of the mixed GF-TTMn synapse in *Drosophila melanogaster* uses acetylcholine as its neurotransmitter. *Eur. J. Neurosci.* **26**, 439–445 (2007).
31. Maimon, G., Straw, A.D. & Dickinson, M.H. Active flight increases the gain of visual motion processing in *Drosophila*. *Nat. Neurosci.* **13**, 393–399 (2010).
32. Tootoonian, S., Coen, P., Kawai, R. & Murthy, M. Neural representations of courtship song in the *Drosophila* brain. *J. Neurosci.* **32**, 787–798 (2012).
33. Llinás, R. & Sugimori, M. Electrophysiological properties of *in vitro* Purkinje cell dendrites in mammalian cerebellar slices. *J. Physiol. (Lond.)* **305**, 197–213 (1980).
34. Gouwens, N.W. & Wilson, R.I. Signal propagation in *Drosophila* central neurons. *J. Neurosci.* **29**, 6239–6249 (2009).
35. Hatsopoulos, N., Gabbiani, F. & Laurent, G. Elementary computation of object approach by wide-field visual neuron. *Science* **270**, 1000–1003 (1995).
36. Sun, H. & Frost, B.J. Computation of different optical variables of looming objects in pigeon nucleus rotundus neurons. *Nat. Neurosci.* **1**, 296–303 (1998).
37. Kohashi, T. & Oda, Y. Initiation of Mauthner- or non-Mauthner-mediated fast escape evoked by different modes of sensory input. *J. Neurosci.* **28**, 10641–10653 (2008).
38. Cisek, P. & Kalaska, J.F. Neural mechanisms for interacting with a world full of action choices. *Annu. Rev. Neurosci.* **33**, 269–298. 10.1146/annurev.neuro.051508.135409 (2010).
39. McPeek, R.M. & Keller, E.L. Superior colliculus activity related to concurrent processing of saccade goals in a visual search task. *J. Neurophysiol.* **87**, 1805–1815 (2002).
40. Cisek, P. & Kalaska, J.F. Neural correlates of reaching decisions in dorsal premotor cortex: specification of multiple direction choices and final selection of action. *Neuron* **45**, 801–814. 10.1016/j.neuron.2005.01.027 (2005).
41. Cisek, P. Cortical mechanisms of action selection: the affordance competition hypothesis. *Phil. Trans. R. Soc. Lond. B* **362**, 1585–1599. 10.1098/rstb.2007.2054 (2007).
42. Burrows, M. & Rowell, C.H.F. Connections between descending visual interneurons and metathoracic motoneurons in locust. *J. Comp. Physiol.* **85**, 221–234 (1973).
43. Rind, F.C. A chemical synapse between two motion detecting neurones in the locust brain. *J. Exp. Biol.* **110**, 143–167 (1984).
44. Gray, J.R., Blincow, E. & Robertson, R.M. A pair of motion-sensitive neurons in the locust encode approaches of a looming object. *J. Comp. Physiol. A Neuroethol. Sens. Neural Behav. Physiol.* **196**, 927–938 (2010).
45. Eaton, R.C., Lee, R.K. & Foreman, M.B. The Mauthner cell and other identified neurons of the brainstem escape network of fish. *Prog. Neurobiol.* **63**, 467–485 (2001).
46. O'Malley, D.M., Kao, Y.H. & Fetcho, J.R. Imaging the functional organization of zebrafish hindbrain segments during escape behaviors. *Neuron* **17**, 1145–1155 (1996).
47. Svoboda, K.R. & Fetcho, J.R. Interactions between the neural networks for escape and swimming in goldfish. *J. Neurosci.* **16**, 843–852 (1996).
48. Bullock, T.H. Comparative neuroethology of startle, rapid escape, and giant fiber–mediated responses in *Neural Mechanisms of Startle Behavior* (ed. R.C. Eaton) 1–13 (Plenum Press, 1984).
49. Trimarchi, J.R. & Schneiderman, A.M. Different neural pathways coordinate *Drosophila* flight initiations evoked by visual and olfactory stimuli. *J. Exp. Biol.* **198**, 1099–1104 (1995).
50. de Vries, S.E. & Clandinin, T.R. Loom-sensitive neurons link computation to action in the *Drosophila* visual system. *Curr. Biol.* **22**, 353–362 (2012).

ONLINE METHODS

Fly stocks. *Drosophila melanogaster* were reared on the standard cornmeal fly food at 22–25 °C and 50% humidity on a 16-h light/8-h dark cycle. Flies were used 2–5 d post-eclosion. Males and females were used for all experiments except where specified. Data were acquired using the following fly stocks: *DL* (wild-type strain from M.H. Dickinson, University of Washington), *R17A04_p65ADZp (attP40); 68A06_ZpGdbd (attP2)* (T. Ngo and A. Jenett, Janelia Farm Research Campus), *w; R17A04_p65ADZp (attP40); pJFRC12-10XUAS-IVS-myr::GFP (su(Hw)attP1), R68A06_ZpGdbd (attP2)/TM6b*[24], *R17A04_p65ADZp (attP40)* (Rubin Lab), *R68A06_ZpGdbd (attP2)* (Rubin Lab), *w+;; pJFRC28-10XUAS-IVS-GFP-p10 (attP2)* (vector as described previously[51], in a wild-type, Canton S, background, M. Heisenberg, University of Würzburg), *UAS-CsChrimson (attP18)*[26], *w;; UAS-P2X2(III), pJFRC28-10XUAS-IVS-GFP-p10 (attP2)*[19,51], *w+;; pJFRC49-10XUAS-IVS-eGFPKir2.1 (attP2)* (a gift from B.D. Pfeiffer, Rubin Lab, Janelia Farm Research Campus), generated by subcloning eGFPKir2.1 from pUAS-EGFP-Kir2.1 (gift of K. Wantanabe and D.J. Anderson, Caltech) 5′ -SalI to 3′ -AvrII into cohesive compatible 5′ -XhoI to 3′ -XbaI sites of *pJFRC2-10XUAS-IVS* (personal communication, B.D. Pfeiffer; and as described previously[24] in a wild-type, *DL* background).

Visual stimuli. Visual stimuli were presented at 768 × 768 resolution on 7-inch diameter back-projection coated hemispheres with DMD projectors modified to run at 360 Hz in grayscale (developed by A. Leonardo and Lightspeed Design; model WXGA 360), driven by MATLAB using the Psychophysics Toolbox extensions[52,53]. Constant velocity, looming stimuli of a black disk expanding on a white background were generated in a custom MATLAB script.

$$\theta_{\text{stim}} = 2\tan^{-1}(r/(vt)) \quad (1)$$

where θ_{stim} is the angular size subtended on the retina over time and r/v is the half size to speed ratio[23]. Distortion from projecting onto a curved surface was corrected by mapping each two-dimensional image to the hemisphere surface. Irradiance differences resulting from projecting on to a curved surface were corrected out to 70° from the center of each hemisphere.

$$\text{pixel correction factor} = \frac{1/\cos(\theta_p)}{1/\cos(70°(\pi/180°))} \quad (2)$$

where θ_p is a pixel's angular distance from the center of the hemisphere, in radians. As a result, maximum irradiance values were 0.01 mW cm^{-2} for black and 2.57 mW cm^{-2} for white as measured at the center of the hemisphere. Individual frame presentations were monitored with a photodiode to synchronize stimulus presentation with data acquisition.

Fly free behavior. Responses of unrestrained flies to computer generated looming stimuli were captured using a dedicated, high-throughput behavioral apparatus (**Supplementary Fig. 1**) that permitted collection of large sample sizes necessary to quantitatively characterize differences in timing and duration of escape behavior. Flies were released one at a time onto a prism via an automated gate. The requirement for flies to walk up a vial, through a tunnel, before release was used to confirm that the wild-type and transgenic flies had no gross motor deficits. When a fly reached the top surface of the prism, a projector and high-speed video camera (Photron SA4) were simultaneously triggered. The triggered projector cast a dark disk stimulus on a white dome placed over the prism, as described in detail above. Stimuli expanded from 15° to 90° at an elevation of 45° and a frontward azimuth bias (±60° for over 90% of flies, as measured from the front of the fly). Only one stimulus was presented per fly; flies failing to takeoff were removed from the platform before release of the next fly. The sequence for testing experimental groups was not randomized; however, all experiments were performed during the 4-h activity peak in the afternoon light cycle. Video was recorded at 6,000 frames per second under infrared (740 nm) lighting. Video data were analyzed manually by recording the frame in which a fly's wings first started to open off its back (start of wing raising and the escape sequence), the frame in which the mesothoracic legs first extended at the femur-tibia joint (start of middle leg extension), the frame in which the wings first moved downwards (start of wing depression and flight) and the frame in which the legs were last touching the ground (takeoff frame, end of the escape sequence) by a technician unbiased to the experimental groups. Wing position (fully raised (≥45°) or not fully raised (<45°)) within 2 ms before takeoff was blindly scored by three separate individuals and averaged across flies. Flies slipping on attempted takeoff (failure to loose tarsal contact with the surface to enable quantification of escape duration) were excluded from the analysis (174 of 2,748 flies were excluded).

CsChrimson activation. Responses of unrestrained flies to CsChrimson[26] activation were captured using the behavioral apparatus describe above. After a single fly was released onto the prism, CsChrimson was activated in experimental (raised on standard cornmeal fly food with 0.2 mM retinal) and control (raised only on standard cornmeal fly food) flies with four 624-nm wavelength LEDs (total irradiance of 500 W m^{-2}, as measured from the location of the fly on the prism). The LEDs remained on for 2 s, however, and experimental flies performed a takeoff in the first 220 ms after the LEDs were triggered. Wing position was not scored for experimental flies having elevated wings before light activation. Control flies were scored for takeoff if it occurred in the 2 s of the light pulse.

Electrophysiology in tethered, behaving animals. Female flies were anesthetized at 4 °C and tethered to stainless steel recording plates at the head and thorax with UV glue (an adapted version of the tethered flight preparation[31]; **Fig. 3a**). The prothoracic legs were removed and the proboscis was secured with a drop of glue to prevent brain movement during the recording. The brain was continuously perfused with extracellular saline[34] containing 103 mM NaCl, 3 mM KCl, 5 mM *N*-Tris (hydroxymethyl)methyl-2- aminoethane-sulfonic acid, 8 mM trehalose, 10 mM glucose, 26 mM $NaHCO_3$, 1 mM NaH_2PO_4, 1.5 mM $CaCl_2$ and 4 mM $MgCl_2$ (osmolarity adjusted to 270–275 mOsm), bubbled with 95% O_2/5% CO_2 and adjusted to a pH of 7.3 held at a constant 22 °C. Collagenase (0.5% in extracellular saline) was locally applied through a patch pipette to disrupt the perineural sheath above the giant fiber cell body. Patch clamp electrodes (3-4.5 MΩ) were filled with intracellular saline[34] containing 140 mM potassium aspartate, 10 mM HEPES, 1 mM EGTA, 4 mM MgATP, 0.5 mM Na_3GTP and 1 mM KCl (osmolarity adjusted to 260-275, pH 7.3). Alexa-568-hydazide-Na (20 µM, Invitrogen) was included in the intracellular saline to verify correct targeting of the GFs. Recordings were acquired in current clamp mode with a MultiClamp 700B amplifier (Molecular Devices), low-pass filtered at 10 kHz, and digitized (Digidata 1440A, Molecular Devices) at 20 kHz. Recordings were deemed acceptable if a high seal resistance was formed before rupture (~8 GΩ), the resting membrane potential was ≤ −55 mV and if flies were able to produce spontaneous leg movements throughout the recording (31 of 86 recordings were excluded). Current injection was held at zero for all recordings and never adjusted to bring the resting membrane potential to a particular resting level. Traces were not corrected for a 13-mV liquid junction potential[34].

During visual stimulus presentation, flies were centered between two hemispheres to permit stimulus presentation on either side of the fly (**Fig. 3a**) for video recordings of fly behavior from the front of the fly. For behavioral video recordings from the side of the fly, one hemisphere was removed. Flies were tethered with an average pitch of −63 ± 4° with respect to the horizon and with offset in roll and yaw limited to ±3° in each direction. All flies were light adapted to a white background for greater than 20 min before the start of the experiment. To probe the GF's response to different looming speeds, looming stimuli expanded from 5° to 90° at three separate r/v ratios and remained at 90 degrees for 1 s. Looming stimuli were presented every 20 s in a randomized order at an elevation of 11° and azimuth location of ±51° with respect to the fly (based on the average pitch).

For ATP/$P2X_2$ receptor stimulation of the GFs, a glass capillary pulled to a 1 µm diameter was positioned on GFP and $P2X_2$ receptor expressing GF dendrites in the ventrolateral protocerebrum (**Fig. 2a**), a major visual output region from the optic lobes[16,22]. ATP (1 mM) was microinjected (2.5–5 psi, 50-ms pulse) under the control of a Picospritzer (Parker Hannifin) at 2-min intervals to permit full recovery to the resting membrane potential between pulses. To test for contributions of voltage gated sodium (tetrodotoxin, 1 µM) and calcium (Cd^{2+}, 100 µM) channels, recordings were made 5 min after bath application of the respective channel inhibitors.

Behavior was monitored with a high-speed video camera (Photron SA4) at 2,000 Hz from the front or 4,000 Hz from the side of the fly. Images and electrophysiology data were synchronously acquired through an MCDL board (Photron). Flies were illuminated by an infrared (850 nm) LED light source and

doi:10.1038/nn.3741

the wingbeat frequency was monitored with a Wingbeat Tachometer (IO Rodeo) containing a high pass (850 nm) filter.

Immunohistochemistry and imaging. Antibody staining was performed on dissected, fixed brains and ventral nerve cords using the following antibodies: rabbit antibody to GFP (1:500, Invitrogen), mouse antibody to NC82 (1:40, Developmental Studies Hybridoma Bank), Alexa Fluor 488 goat antibody to rabbit (1:500, Invitrogen), Alexa Fluor 568 goat antibody to mouse (1:500, Invitrogen). Imaging was performed on a Zeiss LSM 510 confocal microscope under 20× magnification. Data were acquired at a 0.62 × 0.62 µm pixel size and 1-µm-thick *z* section using an 8-bit dynamic range and averaging two successive scans. Maximum intensity projections were generated from the *z* stacks and contrast and brightness were optimally adjusted. Using this technique, we successfully repeated selective GFP labeling of the GFs using our GF split-GAL4 driver line in 18 of 18 flies.

Modeling. Neural delays and angular thresholds in free behavior data were estimated according to previously established methods[23,35]. The median time of takeoff (T_{ttc}) or time of wing elevation (W_{ttc}), with respect to time of contact (TTC), across r/v values was fit with a linear regression.

$$T_{ttc} \text{ or } W_{ttc} = -\alpha(r/v) + \delta \tag{3}$$

The y intercept, δ, represents the neural delay following an instantaneous stimulus. This delay was used to plot the angular threshold (θ_{thresh}) per fly across r/v.

We then built a model for our free behavior data centered around two separate takeoff pathways, each with corresponding θ_{thresh} and escape behavior duration distributions, whose parameters were derived from cases in which only the GF (GF spiking trials or GF Chrimson activation) or the alternate pathway (GF Kir trials) was active. The value α from equation (3) was first used to model the average θ_{thresh}.

$$\theta_{thresh} = 2\tan^{-1}(1/\alpha) \tag{4}$$

whereas the s.d. in θ_{thresh} was modeled by the linear regression of the s.d. of the initiation of the behavior (T = time of spike for GF pathway and time of wing raising for alternate escape pathway; **Supplementary Fig. 6a**,**b**)

$$\sigma_T = \rho(r/v) \tag{5}$$

using

$$\sigma_\theta = (2\rho)/(1+\alpha^2) \tag{6}$$

We found that this method provided a good fit for θ_{thresh} of long and GF-silenced wing raising and takeoffs. However, it provided an incomplete description of spiking response of the GF and θ_{thresh} was better described by a normal distribution after log transforming the data (**Supplementary Fig. 6c**). This suggests that although the angular threshold model provides a good estimate of stimulus parameters driving the decision to escape in the absence of the GF, it may not completely describe the response of the GF.

Action selection between the two circuits was modeled on a per fly basis in which a θ_{thresh} was randomly chosen from the fitted distributions. Wing elevation then occurred at the respective fixed delay (δ from equation (3)), with an addition 1 ms to account for time for spike propagation to behavior initiation in GF responses) after θ_{thresh}, and was followed by takeoff at a variable duration (sampled from the respective distributions in **Fig. 2e**). The winning pathway was chosen based on the first to trigger a takeoff, and the GF pathway could interrupt wing raising of the other pathway to result in an earlier takeoff. To account for a decreased likelihood to elicit an escape at smaller r/v, we added in a response likelihood across r/v, as measured in control flies (probability of escape = 0.29, 0.56, 0.74, 0.84 and 0.85 for r/v = 8, 14, 40, 70 and 140 ms, respectively).

Damselfly studies. Male and female adult wild-type *Drosophila melanogaster* were taken from the lab colony and released into a 3 × 3 × 4-foot clear plastic box inside an environmental room that was illuminated to outdoor conditions (~5 mW cm^{-2}) and wallpapered with natural garden scenes. Temperatures in the room cycled between 31 °C during the day and 19 °C overnight. *Enallagma* and *Ischnura* damselflies were wild-caught from two pond sites in Ashburn, Virginia, and kept on ice 1–4 h before experiments. The box was populated with 10–15 damselflies and 4–8 bottles (~500) of *Drosophila* per experimental period. Animals flew freely within the confines of the box and were allowed to remain in the box for 1–3 d of data collection. Two orthogonal high-speed cameras (Photron SA1) were trained on the interior volume of the box, and the two walls opposite the cameras were lined with plastic mesh to provide the damselflies with appropriate depth cues. Videos were recorded at 1,000 frames per second using Photron software. Wild-caught damselflies attacked flies as they perched on the wall of a large population cage by first positioning themselves at the same elevation as a targeted fly, then darting forward and grabbing the fly with all six legs. For analysis, damselfly head, damselfly abdomen and fly body centroid points were marked manually in each video frame using DLTdv3 software by Ty Hedrick. Analysis of these three-dimensional trajectories was then performed using custom programs in MATLAB (MathWorks). Damselfly trajectories were rotated into the same reference frame based on initial fly coordinates and sorted into 'capture' and 'escape' events based on outcome. A damselfly approach was considered a capture if the damselfly successfully plucked the fly from the wall and consumed it. An approach was considered an escape if the fly took off from the wall before the damselfly reached it and the fly had been targeted by the damselfly. To be considered as targeting a fly, the damselfly had to be oriented toward the fly (angle between damselfly body axis and the line connecting damselfly and fly center of masses < 35°) and its center of mass velocity had to be moving toward the fly (angle between damselfly velocity vector and the line connecting damselfly and fly center of masses < 35°). Trajectories were then aligned in time by aligning the minimum damselfly to fly distance to obtain the lowest residuals (time = 0 ms in **Fig. 6b**,**c**). To determine the actual expansion profile of the damselfly on the fly's eye, we calculated the widest extent of the damselfly's head and body visible by the fly in each frame of video ($2r$). We assumed a fixed ratio for the width of the damselfly head relative to the body, and that the head remained perpendicular to the body. The angular size of the damselfly head projected onto the fly's eye (θ_{exp}) in each frame is then

$$\theta_{exp} = 2\tan^{-1}(r/d) \tag{7}$$

where d is the Euclidean distance between the damselfly and the fly. To model the measured expansion profile, we then fit the nonlinear change in θ_{exp} over time for either the average damselfly trajectory for each event type (**Fig. 6b**,**c**) or each individual damselfly trajectory (**Fig. 6d–f**) using the following equation, which describes the time-varying visual angle, θ_{mod}, of an object with largest dimension $2r$ approaching the fly on a collision course with initial velocity, v, and acceleration, a.

$$\theta_{mod} = 2\tan^{-1}\left(\frac{r}{D_0 - vt - 0.5at^2}\right) \tag{8}$$

Our two varying parameters in this model were acceleration, a, and the size-to-speed ratio (r/v). For each individual trajectory, D_0 was a constant representing the starting distance between the damselfly and fly 85 ms before escape or capture, and r was a constant representing real-world half-size of the damselfly's head, $2r$. Velocity was calculated by dividing the half size of the damselfly's head by our parameterized size to speed ratio. We calculated the residuals between θ_{mod} and θ_{exp} for θ_{mod} calculated with values of a ranging from −0.003 to 0.003 m s^{-2} and size-to-speed ratios ranging from 0–200 ms.

Data analysis and statistics. Data analysis was performed using custom Matlab scripts. All data, except those from animals excluded as explained above, were analyzed. Prior to statistical testing, data were tested for normality with a Kolmogorov-Smirnov test and the appropriate non-parametric test was chosen if data were not normally distributed. All statistical tests and significance levels for data comparisons are specified in the results section of the text or figure captions and are two-sided unless specified otherwise. Variance is displayed on all figures as s.d., s.e., 95% confidence interval or 25–75th percentile, as specified

in the figure caption. Variance between groups was not statistically compared. Adjustments for multiple comparisons were conducted as stated in the figure captions and text.

For free behavior studies, measurements of the escape sequence duration were fit with a Gaussian mixture model by the Expectation Maximization algorithm with initial conditions set for equally weighted Gaussian distributions. The number of Gaussians present in each fit were determined by finding the minimum Bayesian information criterion among the best fit Gaussian mixture models of one to five Gaussians. Least-squares linear regression was used to fit lines to the percent GF short response by log (r/v), to the survival percentage by percent GF short among different genotypes, and to all behavioral and modeled mean wing elevation timing takeoff timing and θ_{thresh} data, and R^2 values are as specified in the figure captions.

51. Pfeiffer, B.D., Truman, J.W. & Rubin, G.M. Using translational enhancers to increase transgene expression in *Drosophila*. *Proc. Natl. Acad. Sci. USA* **109**, 6626–6631 (2012).
52. Brainard, D.H. The psychophysics toolbox. *Spat. Vis.* **10**, 433–436 (1997).
53. Pelli, D.G. The VideoToolbox software for visual psychophysics: transforming numbers into movies. *Spat. Vis.* **10**, 437–442 (1997).

doi:10.1038/nn.3741